Journal of Analytical and Applied Pyrolysis 157 (2021) 105167

Contents lists available at ScienceDirect

Journal of Analytical and Applied Pyrolysis

journal homepage: www.elsevier.com/locate/jaap

Pyrolysis kinetics of wildland vegetation using model-fitting methods☆

Elham Amini [a], Mohammad-Saeed Safdari [a], Nathan Johnson [a], David R. Weise [b], Thomas H. Fletcher [a,*]

[a] Department of Chemical Engineering, Brigham Young University, Provo, Utah, 84602, USA
[b] USDA Forest Service, PSW Research Station, Fire and Fuels Program, Riverside, CA, 92507, USA

ARTICLE INFO

Keywords:
Pyrolysis
Kinetic
Thermogravimetric analysis
DAE model
Live and dead vegetation

ABSTRACT

Slow-heating pyrolysis experiments of 14 plant species native to forests in the southern United States were conducted in a TGA to find the kinetic parameters for slow pyrolysis of all live and air-dried plant samples. Kinetic coefficients were determined from the data using model-fitting methods, resulting in single kinetic parameters for the entire pyrolysis process which can be used by wildland fire modelers. The model forms explored here are a simple one-step model and single and multiple reaction distributed activation energy (DAE) models. The mass loss and derivative mass loss data were fitted simultaneously at heating rates of 10, 20, and 30 °C min^{-1} to find kinetic parameters for these model forms.

The multiple-reaction DAE model gave the best fit to the pyrolysis data at multiple heating rates when multiple peaks were observed. The multiple pyrolysis peaks were attributed to decomposition of hemicellulose, cellulose, and lignin, based on literature observations for biomass. The order of activation energies for pyrolysis of all plant species indicated that hemicellulose and extractives decompose more readily than cellulose and finally lignin.

1. Introduction

Prescribed burning in the southern United States is an important tool used by land managers to accomplish several objectives such as wildlife habitat management, hazardous fuel reduction, maintenance of critical military training areas, control of insects and disease, improved grazing, maintenance of fire-dependent species and plant communities and management of competing vegetation [1]. In order to refine fire application to achieve desired fire characteristics and reduce undesirable fire characteristics, an improved understanding of the main processes related to pyrolysis and ignition is needed for the heterogenous fuel beds of live and dead vegetation [2].

The pyrolysis of major biomass components such as cellulose, hemicellulose and lignin has been studied in detail [3–8]. However, the study of these components is not sufficient to understand the pyrolysis behavior of plant species during wildland fires [9]. Plant species are a combination of these biopolymers, and the presence of each component affects the pyrolysis of others. While there are general descriptions of the compositional makeup of plants for combustion and smoke emissions purposes, it has long been recognized that plants differ chemically and physically in many ways that contribute to differing combustion behavior [10–14]. Kinetic models are needed to describe the pyrolysis behavior of a plant which contains different components.

As biomass is heated, moisture is first released at temperatures below 150 °C. At low heating rates, two distinct peaks in the pyrolysis rate are often observed at 250–350 °C and 300–450 °C, which are attributed to the degradation of cellulose and hemicellulose. A broad peak is also often modeled ranging from 200 to 600 °C that is thought to represent a combination of pyrolysis of cellulose, hemicellulose, and lignin (see for example [4,7,15]).

Thermogravimetric Analyzer (TGA) is the most common tool used by many researchers to study the pyrolysis kinetics of woody biomass. Thermogravimetric/differential thermogravimetry (TG/DTG) experiments can be either isothermal or non-isothermal. Non-isothermal methods are most commonly used for pyrolysis, since pyrolysis always starts during the heating period [16–19]. At a constant heating rate, time and temperature are related through:

$$T = \beta\, t + T_0 \quad (1)$$

where t is time, β is the heating rate, T is the temperature, and T_0 is the initial temperature.

Global devolatilization models are generally used to describe

☆ This manuscript was prepared, in part, by a U.S. Government employee on official time, is not subject to copyright and is in the public domain.

* Corresponding author at: 330 EB, BYU, Provo, UT, 84602, USA.
E-mail address: tom_fletcher@byu.edu (T.H. Fletcher).

https://doi.org/10.1016/j.jaap.2021.105167
Received 25 January 2021; Received in revised form 17 March 2021; Accepted 13 April 2021
Available online 14 May 2021

biomass pyrolysis due to the complexity of the solid-phase reactions. There are three types of global devolatilization kinetic models: one-step models, two-competing-step models, and distributed activation energy (DAE) models. In each model, the number of kinetic pathways that reaction can take determines the number of steps. These models have been used to study pyrolysis kinetics for a variety of biomass fuels [4,20,21].

The slow and fast pyrolysis characteristics of live and dead vegetation native to the southern United States and the analysis of pyrolysis products and the effect of temperature and heating rates on the distribution of pyrolysis products have been measured in detail [22–27]. In addition, the kinetics of pyrolysis using iso-conversional methods and the dependence of activation energy on conversion were explored, and kinetic parameters as a function of conversion were reported [28]. However, since several current physical models of wildland fire use a single kinetic parameter obtained from global kinetic models, a study was performed to find single kinetic parameters for selected wildland plants based on these global kinetic models.

In this work, the kinetics of pyrolysis of 14 plant species native to the southern United States using global kinetic models were studied using simple model forms, including a simple one-step model as well as single- and multiple-reaction DAE models.

2. Experimental

2.1. Material

Amini et al. [22,28] studied the slow-heating pyrolysis of 14 different plant species native to the southeastern United States forests. These plant species were selected to represent the range of live wildland fuels that commonly occur in wildland fires in this region which accounts for approximately 2/3 of the area (4.7 million ha) treated with prescribed fire in the U.S. annually [29]. The plants were grown in nurseries in the region and shipped overnight to the fire laboratory at Brigham Young University in Utah. Foliage at two moisture levels, live and air-dried, were used in the TGA apparatus. A portion of the plants were cut from the roots and allowed to air dry for a minimum of one week to reach a moisture content less than 10 wt%; these air-dried samples are referred to in this paper as dead since they are below the commonly assumed moisture content for dead plants of 30 wt%. While moisture content of the sample and plant species were the two experimental factors studied, it was possible to study the effect of aging (weathering) for one of the species. The primary dead fuel in the pine forests of the southeastern U.S. is the cast foliage (pine straw) from the pine trees. Because longleaf pine is an evergreen tree, its living needles are retained on the plant for one or two growing seasons [30,31] and then abscised. The foliage loses its characteristic green color and the protective waxy cuticle begins to weather on the forest floor. Table 1 lists the plant species used in the pyrolysis experiments, classified into four growth types: shrub, palm, tree, and grass. The elemental analysis and the component analysis (i.e., cellulose, hemicellulose, lignin, and details of extractives) of these plant species were published by Matt et al. [14] and included with permission in the Supplementary Material (**Tables S1-S3**).

Table 1
List of plants used in pyrolysis experiments.

Common name	Scientific name	Growth form	Leaf shape
Inkberry	*Ilex glabra (L.) A. Gray*	Shrub	Elliptical
Yaupon	*Ilex vomitoria Aiton 'Schelling Dwarf'*	Shrub	Elliptical
Fetterbush	*Lyonia lucida (Lam.) K. Koch*	Shrub	Elliptical
Wax myrtle	*Morella cerifera (L.) Small*	Shrub	Elliptical
Darrow's blueberry	*Vaccinium darrowii Camp "Rosa's Blush"*	Shrub	Elliptical
Sparkleberry	*Vaccinium arboreum Marshall*	Shrub	Elliptical
Swamp bay	*Persea palustris (Raf.) Sarg.*	Shrub	Elliptical
Dwarf palmetto	*Sabal minor (Jacq.) Pers.*	Palm	Palmate
Saw palmetto	*Serenoa repens (W. Bartram) Small*	Palm	Palmate
Water oak	*Quercus nigra L.*	Tree	Elliptical
Live oak	*Quercus virginiana Mill.*	Tree	Elliptical
Longleaf pine foliage	*Pinus palustris Mill.*	Tree	Linear
Longleaf pine litter (pine straw)	*Pinus palustris Mill.*	Tree	Linear
Little bluestem	*Schizachyrium scoparium (Michx.) Nash*	Grass	Linear
Wiregrass	*Aristida stricta Michx.*	Grass	Linear

2.2. Thermogravimetric experiments

Slow-heating pyrolysis experiments were performed in a thermogravimetric (TGA-DSC METTLER TOLEDO)[1] in Helium with a flow rate of 50 mL min^{-1} [22,28]. For each experiment, an approximate 6 mg sample of leaf or needles was placed in the platinum 30 μL crucible. Samples were cut from the leaf (or needle) portion of the live or dead samples and placed directly in the crucible within a few seconds. Three replications were performed for each plant species using linear heating rates of 10, 20 and 30 °C min^{-1} (9 experimental runs) with a final temperature of 800 °C. To exclude buoyancy effects, a blank experiment was conducted before each experiment. Small particle sizes (0.5−1 mm) were used in order to ensure kinetic control and eliminate heat and diffusion transfer problems.

[1] The use of trade or firm names in this publication is for reader information and does not imply endorsement by the U.S. Department of Agriculture of any product or service.

3. Kinetic modeling

Biomass pyrolysis depends on the conversion, residual mass, heating rate, and temperature. The mass loss and derivative mass loss data were fitted simultaneously at heating rates of 10, 20, and 30 °C min^{-1} to find kinetic parameters.

3.1. Simple one-step model

Biomass pyrolysis is often described by the following simple reaction:

$$\text{Solid} \rightarrow \text{Volatiles} + \text{Char} \quad (2)$$

The simple one-step model is based on the Arrhenius reaction form. Many researchers have used this Arrhenius model in computational fluid dynamics (CFD) codes [32–34]. The simple first-order pyrolysis model is:

$$\frac{dV}{dt} = A\exp\left(-\frac{E}{RT}\right)(V_\infty - V) \quad (3)$$

where A and E are Arrhenius kinetic coefficients, t is time, T is the particle temperature, R is the Arrhenius constant, V is the normalized mass of volatiles, and V_∞ is the final value of V.

3.1.1. DAE models

The distributed activation energy (DAE) model was originally proposed by Vand [35] and has been applied to different complex reactions [21,36–41]. This model assumes that the decomposition of biomass occurs through a variety of reactions that have a range of activation energies. The activation energy distribution function representing the range of activation energies is usually taken to be a Gaussian distribution. The DAE approach is therefore similar to iso-conversional techniques, except that the change in activation energy with conversion uses a model form instead of curve-fit at each extent of conversion. In this

study, two forms of DAE were used: (1) the single-reaction DAE model, and (2) the multi-reaction DAE model.

3.1.1.1. Single-reaction DAE model. The single-reaction DAE model is shown in Eq. 4. A mean and standard deviation of the activation energy must be specified along with a single pre-exponential factor. The shape of the distribution function is assumed to be Gaussian. The original formulations of the DAE model used parallel reaction rates, so that all activation energies could participate in the reaction at any time [35,39]. However, since reactions with the lowest activation energies generally participate in the reaction first, the series form of the DAE model proposed by Grant et al. [42] is used, which is much more computationally efficient and physically more realistic. The series reaction formulation calculates the effective activation energy as a function of the extent of reaction based on a Gaussian distribution, as follows:

$$\frac{dV}{dt} = A\exp\left(-\frac{(E_a + \sigma_E Z)}{RT} \right)(V_\infty - V) \tag{4}$$

$$Z = erfinv[1 - 2(V_\infty - V)] \tag{5}$$

where σ_E is the standard deviation for the activation energy distribution, E_a is the mean activation energy, Z is an inverse cumulative Gaussian distribution of activation energies based on fuel conversion, R is the gas constant, V is the normalized mass of volatiles, V_∞ is the final value of V, and *erfinv* is the inverse of the error function.

3.1.1.2. Multiple-Reaction DAE model. According to the DAE model, a plant sample consists of multiple pseudocomponents, where a pseudocomponent is a group of reactive species that show similar reactivity. Each pseudocomponent is composed of a theoretically infinite number of fractions with different activation energies that usually follow a Gaussian distribution. A series formulation of the first-order DAE model is assumed for each pseudocomponent, which defines the time and temperature dependence of the released volatiles, *Vj*:

$$\frac{dV_j}{dt} = A\exp\left(-\frac{(E_{aj} + \sigma_{Ej} Z_j)}{RT} \right)(V_{\infty j} - V_j) \tag{6}$$

$$Z_j = erfinv[1 - 2(V_\infty - V_j)] \tag{7}$$

where σ_{Ej}, E_{aj}, Zj, Vj, and $V_{\infty j}$ are the standard deviation for the activation energy distribution, the mean activation energy, the distribution based on fuel conversion, normalized mass of volatiles, and the final value of *Vj* for the pseudocomponent *j*, respectively. The resulting final reaction rate curve is the weighted sum of the individual d*Vj*/d*t* rates:

$$\frac{dV}{dt} = \sum \frac{dV_j}{dt} \tag{8}$$

$$V_\infty = \sum V_{\infty j} \tag{9}$$

The final volatiles yield of any pseudocomponent is V_j/V_∞.

4. Model evaluating methods

To compare the predicted values from model fitting methods and experimental data obtained from slow pyrolysis of all live and dead plant species in TGA, the root mean square error (RMSE) and mean absolute error (MAE) values were calculated as follows:

$$RMSE = \sqrt{\frac{\sum_{i=1}^{n} (P_i - E_i)^2}{n}} \tag{10}$$

$$MAE = \frac{1}{n}\sum_{i=1}^{n} |P_i - E_i| \tag{11}$$

where P_i is the predicted value from the model, E_i is the experimental data point, and n is the number of employed experimental data points [43].

5. Statistical analysis

For statistical analysis, the ANOVA (Analysis of Variance) data analysis tool in Microsoft Excel 2017 was used [44]. All the results of this study are the average of three replications, and the error bars represent the ±90 % confidence intervals for three experiments. The 90 % confidence intervals (α = 0.1) using the *t*-value table are calculated as follows:

$$\mu = \bar{x} \pm t_{(\alpha,n-1)} \times \left(\frac{s}{\sqrt{n}}\right) \tag{12}$$

where $\bar{x}$ is the average value of the replications, s is standard deviation, n is the number of replications, $t_{(\alpha,n-1)}$ is the *t*-value which is equal to 2.92.

6. Results and discussion

6.1. Completion temperature

The completion temperature has been extensively used by many researchers to characterize pyrolysis and combustion properties of solid fuels [5,45,46]. The temperature where the normalized rate of decomposition decreases consistently to less than 1% min^{-1} is defined as the completion temperature [5]. The pyrolysis completion temperature was determined for both the live and dead plant species at all three heating rates of 10, 20, and 30 °C min^{-1}; the results for the live samples are presented in Fig.1. Similar results for the dead samples are given by Amini [26].

The pyrolysis completion temperature varied between 381 and 473 °C, with little bluestem grass having the lowest completion temperature and inkberry having the highest. The colors in Fig. 1 represent the growth form indicated in Table 1. The grasses and the pine needles had the lowest completion temperature, and the shrubs had the highest completion temperature. The pyrolysis completion temperature may possibly be related to the propensity of the plant species to burn; plant species with low pyrolysis completion temperatures would finish burning earlier in a fire scenario.

The effect of heating rate on completion temperature is also shown in Fig. 1; increasing heating rate increased the completion temperature. For example, increasing heating rate from 10 to 30 °C min^{-1} increased the completion temperature from 458 to 473 °C and from 361 to 381 °C for inkberry and little bluestem grass, respectively. Pyrolysis at higher heating rates occurs in shorter reaction times which results in the decomposition of sample at higher temperature [47,48]. It is expected that the completion temperature will continue to rise at higher heating rates.

The completion temperature was also compared between live and dead samples (Fig. 2). Little bluestem grass, yaupon, and fetterbush had almost the same completion temperature between live and dead samples. Most of the species such as live oak, water oak, wax myrtle, sparkleberry, wire grass, inkberry, Darrow's blueberry, and saw palmetto had higher completion temperature for live samples, showing that these species became more combustible after drying.

For longleaf pine, swamp bay, and dwarf palmetto, the completion temperature was higher for dead samples, showing that these plant species may have become slightly less combustible after drying. Comparing the results for longleaf pine revealed that, aging increased the completion temperature and made the fuel less combustible. This could be caused by lower amount of extractives in pine straw, which pyrolyze at low temperatures and have been reported to have catalytic effects on pyrolysis [6].

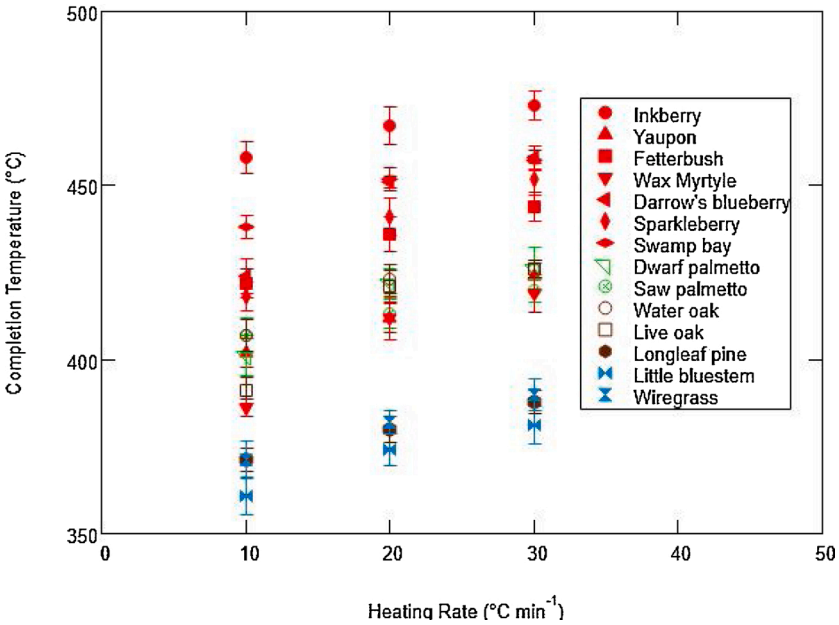

Fig. 1. The completion temperature for all live plant species at heating rates of 10, 20, and 30 °C min^{-1}. Error bars represent the 90 % confidence intervals based on three samples.

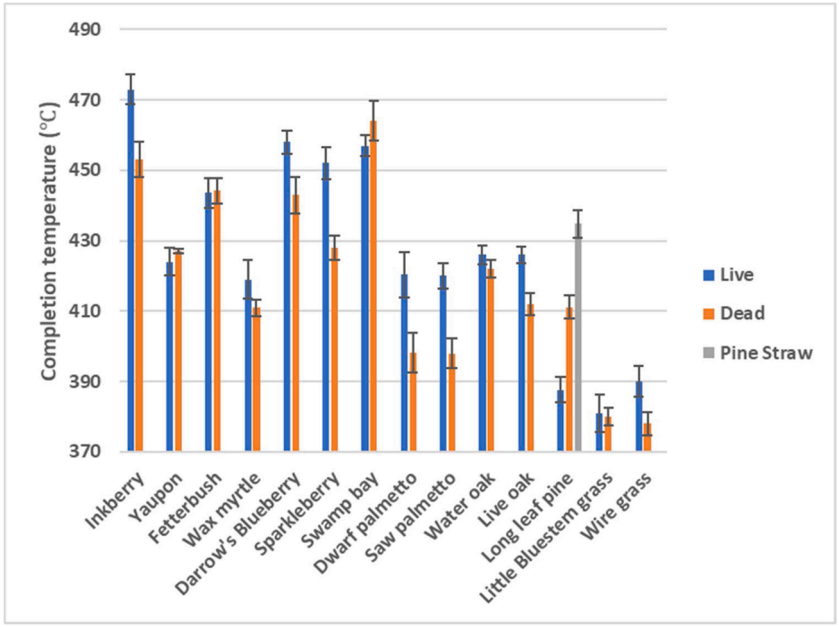

Fig. 2. Completion temperature for all live and dead plant samples at heating rate of 30 °C min^{-1}. Species order is the same as in Table 1 to permit grouping by growth type.

6.2. Simple one-step model

As recommended by Hillier et al. [49], the cumulative mass and the derivative of the mass from all heating rates of 10, 20, and 30 °C min^{-1} were fitted simultaneously to the first-order single reaction model. All fits were performed in Excel using the simple Euler method to integrate the differential equations using the exact time points of the TGA data. Representative curve-fits of the TGA and DTGA single peak and multiple peak pyrolysis data for live little bluestem grass and live water oak using the simple one-step model are presented in Fig. 3. Complete details are given by Amini [26] and are shown in the Supplementary Material (**Fig. S1**).

The values of activation energies and pre-exponential factors for the pyrolysis zone (first peak after the drying zone) of each plant species were determined using the combined data from the experiments at three constant heating rates of 10, 20, and 30 °C min^{-1}, and the results are presented in Table 2 and Fig. 4. For live samples, activation energies obtained from the simple one-step model were in the range of 47.7 to 76.9 kJ mol^{-1}. Yaupon had the lowest activation energy with a value of 47.7 ± 2.8 kJ mol^{-1}. The highest activation energy with a value of 76.9 ± 2.1 kJ mol^{-1} were obtained from pyrolysis of saw palmetto. For dead samples, activation energies were in the range of 47.1 to 76.6 kJ mol^{-1}. The lowest activation energy for dead samples (47.1 ± 2.4 kJ mol^{-1}) was obtained from pyrolysis of yaupon. Dead saw palmetto had the highest activation energy (76.6 ± 1.2 kJ mol^{-1}) of all the dead samples. Among all plant species, dwarf palmetto exhibited the largest statistical

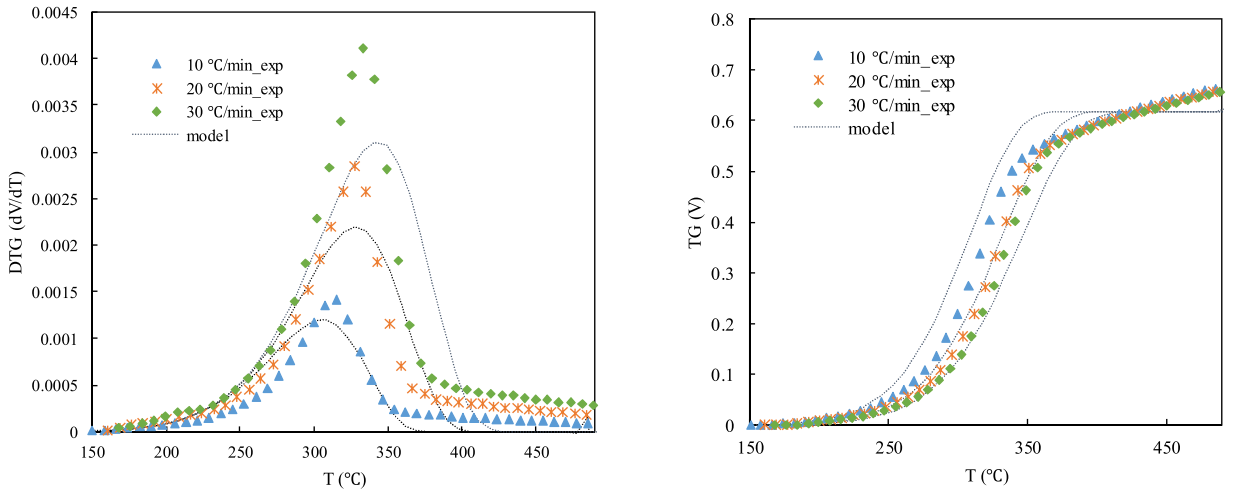

(a) Little bluestem grass (live)

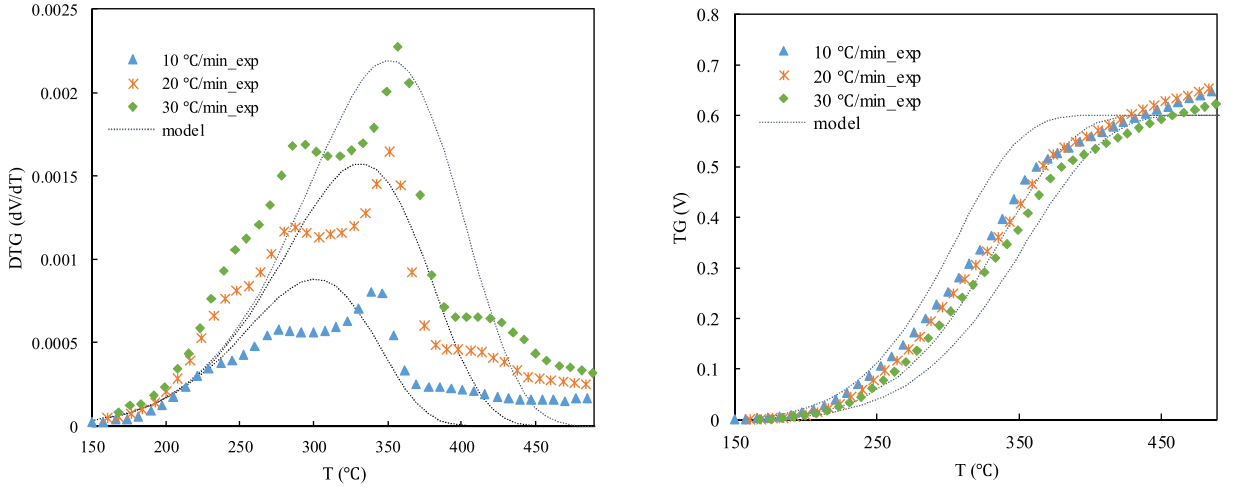

(b) Water oak (live)

Fig. 3. Comparison of simple one-step model curve-fit with TG and DTG curves for (a) live little bluestem grass and (b) live water oak at the heating rates of 10, 20, and 30 °C min^{-1}.

difference in activation energy value (5 kJ mol^{-1}, absolute) between the live and dead samples ($P < 0.05$), which is less than a 10 % difference from the live sample value. Wax myrtle and saw palmetto had the lowest difference in activation energy value (0.3 kJ mol^{-1}) based on simple one-step model between live and dead samples (less than 0.5 % of the live value).

6.3. Single-Reaction DAE model

Using the DAE model with one set of coefficients, the cumulative mass data and the derivative of the mass from the heating rates of 10, 20, and 30 °C min^{-1} were fitted simultaneously in a manner similar to Hillier et al. [49]. Representative curve-fits of the TGA and DTGA single peak and multiple peak pyrolysis data for live little bluestem grass and live water oak using the single-reaction DAE model are presented in Fig. 5. Complete results are shown in the Supplementary Material (**Fig. S2**).

The DAE model matched the DTG peaks fairly well for the single peak curves (Fig. 5a), but did not agree as well with the multi-peak data (bottom left panel). The values of E_a, σ_E, and A for the pyrolysis zones (after drying zone) of each plant species were determined using the combined data from the experiments at three constant heating rates of 10, 20, and 30 °C min^{-1}. The resulting coefficients determined for each plant species are presented in Table 3.

For live samples, activation energies obtained from the single-reaction DAE model were in the range of 123.7 – 270.1 kJ mol^{-1} as shown in Fig. 6. Yaupon had the lowest activation energy with a value of 123.7 ± 5.8 kJ mol^{-1}. The highest activation energy (270.1 ± 4.8 kJ mol^{-1}) was obtained from pyrolysis of saw palmetto. For dead samples, activation energies were in the range of 129.1 – 266.7 kJ mol^{-1}. The lowest activation energy with a value of 129.1 ± 1.3 kJ mol^{-1} was obtained from pyrolysis of yaupon. Saw palmetto had the highest activation energy with a value of 266.7 ± 2.4 kJ mol^{-1}. Among all plant species, pine straw exhibited the largest difference in activation energy value (15.6 kJ mol^{-1}) between the live and dead samples. The next largest differences in activation energies were observed between live and dead samples of sparkleberry (5.5 kJ mol^{-1}) and wax myrtle (5.3 kJ mol^{-1}). Water oak had the lowest difference (0.1 kJ mol^{-1}) in activation energy values based on the single-reaction DAE model between live and dead samples.

Table 2
Kinetic coefficients (mean values of three replicates) obtained from the simple one-step model for each plant species (the 90 % confidence intervals are reported in the parentheses).

Species	E_a (kJ mol^{-1})		Log_{10} A (s^{-1})		V_∞ (normalized)	
	Live	Dead	Live	Dead	Live	Dead
Darrow's blueberry	50.2 (4.4)	51.0 (4.6)	2.23 (0.47)	1.87 (0.25)	0.62 (0.02)	0.62 (0.03)
Dwarf palmetto	54.3 (4.2)	59.3 (6.7)	4.29 (0.86)	3.55 (0.93)	0.62 (0.04)	0.63 (0.02)
Fetterbush	59.9 (4.3)	61.6 (4.2)	2.18 (0.31)	2.41 (0.20)	0.60 (0.03)	0.61 (0.04)
Inkberry	50.6 (4.4)	53.5 (4.5)	1.89 (0.09)	2.64 (0.41)	0.60 (0.03)	0.61 (0.01)
Live oak	51.8 (4.5)	55.3 (3.7)	2.86 (0.20)	2.75 (0.09)	0.55 (0.04)	0.56 (0.06)
Little bluestem grass	58.2 (3.9)	60.1 (7.4)	4.39 (0.30)	4.16 (0.11)	0.60 (0.04)	0.60 (0.01)
Longleaf pine foliage	65.2 (5.3)	61.6 (5.7)	2.49 (0.01)	2.29 (0.02)	0.63 (0.04)	0.61 (0.03)
Longleaf pine litter	–	70.7 (7.2)	–	4.29 (0.13)	–	0.64 (0.03)
Saw palmetto	76.9 (3.5)	76.6 (2.0)	3.47 (0.23)	3.25 (0.14)	0.55 (0.03)	0.55 (0.05)
Sparkleberry	53.2 (4.6)	55.6 (4.8)	2.15 (0.12)	2.51 (0.25)	0.56 (0.−3)	0.56 (0.01)
Swamp bay	54.1 (5.6)	58.4 (7.2)	2.83 (0.22)	2.82 (0.14)	0.61 (0.06)	0.59 (0.02)
Water oak	50.6 (3.9)	52.9 (4.9)	2.42 (0.11)	3.23 (0.12)	0.60 (0.03)	0.60 (0.02)
Wax myrtle	66.7 (5.3)	66.4 (1.8)	2.40 (0.12)	2.20 (0.17)	0.50 (0.02)	0.51 (0.02)
Wire Grass	74.6 (5.1)	72.2 (2.2)	4.54 (0.11)	4.45 (0.27)	0.66 (0.03)	0.67 (0.03)
Yaupon	47.7 (3.1)	47.1 (4.0)	2.37 (0.15)	2.59 (0.13)	0.58 (0.02)	0.57 (0.03)

6.4. *Multiple-Reaction DAE model*

A different number of reactions corresponding to the number of DTG peaks and shoulders were considered for each plant species. Note that the DTG peaks occurred at different temperatures for each plant type (Fig. 7). For Darrow's blueberry, fetterbush, live oak, saw palmetto, sparkleberry, water oak, wax myrtle, wire grass, and yaupon, the DTG curves at a heating rate of 30 °C min^{-1} have two main peaks at 250–320 °C and 320–355 °C followed by a side peak or shoulder around 420 °C. Based on the biomass pyrolysis literature, the first peak can be attributed mainly to hemicellulose decomposition. Cellulose decomposition is thought to form two groups of reactions (second and third peaks) due to the more complex structures of these plant species than pure cellulose. Water oak also has a shoulder around 240 °C, which may be attributed to the decomposition of extractives. The decomposition of components obviously depends on the structure of the plant species. The plant species with more complex structures are more difficult to decompose.

For all plant species, lignin is thought to decompose over a wide range of temperatures (100–600 °C), overlapping the other peaks, so that each reaction modeled likely describes some portion of lignin degradation. Dwarf palmetto exhibited a main pyrolysis peak around 330 °C and a side peak around 410 °C, both of which are likely attributed to cellulose decomposition. The two side shoulders around 220 °C and 290 °C are likely attributed to the extractives and hemicellulose decomposition, respectively. Inkberry exhibited a main peak around 290 °C. The two peaks around 360 and 430 °C and a shoulder around 450 °C are attributed to the cellulose decomposition. A side shoulder around 230 °C is related to the decomposition of extractives.

For little bluestem grass, the two cellulose peaks and the hemicellulose peak observed for most of the plant species are highly merged around 320 °C, which may be due to the catalytic activity of the mineral content for this species. Swamp bay has a main peak and a shoulder that occurred around 355 °C and 410 °C, respectively. Two observed shoulders around 240 °C and 325 °C are mainly attributed to the extractives and hemicellulose decomposition, respectively. For longleaf pine foliage and pine straw, the main pyrolysis peak occurred around 370 and 355 °C, respectively, which is attributed to the cellulose decomposition. Both of these samples also showed a side peak between 410–430 °C. Two observed shoulders between 230 and 350 °C are attributed to the extractives and hemicellulose decomposition.

Similar DTG curves and the same number of reactions were observed for both longleaf pine foliage and pine straw. However, a shift in the temperatures of the peaks in the DTG curve of pine straw was observed, which could be attributed to the lower amount of extractives in pine straw (which have been shown to have catalytic effects during pyrolysis). Swamp bay exhibited a similar pyrolysis behavior to longleaf pine foliage.

Even though the peaks and shoulders for all plant species are mainly attributed to the decomposition of main components (e.g. cellulose,

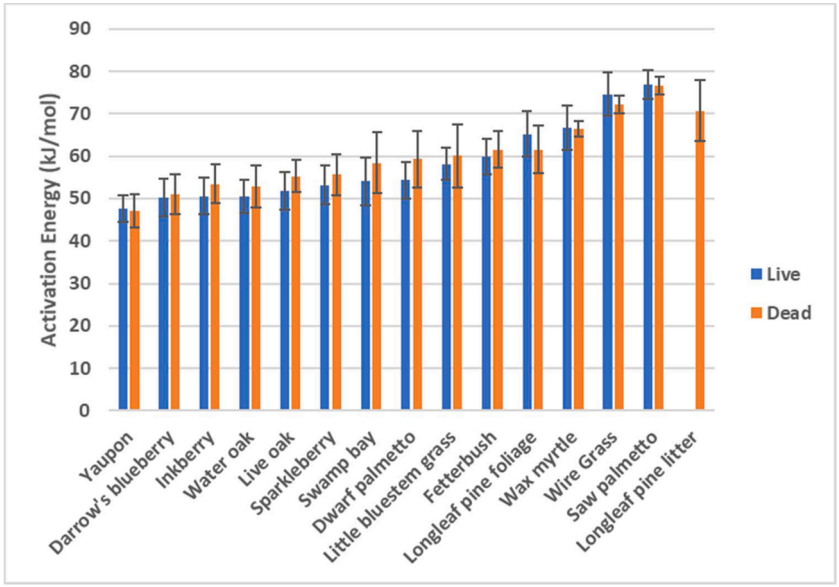

Fig. 4. Comparison of activation energies from the simple one-step model curve-fit with TG and DTG curves at heating rates of 10, 20, and 30 °C min^{-1}. Error bars represent the 90% confidence intervals. Activation energies are shown in order of the live sample activation energy.

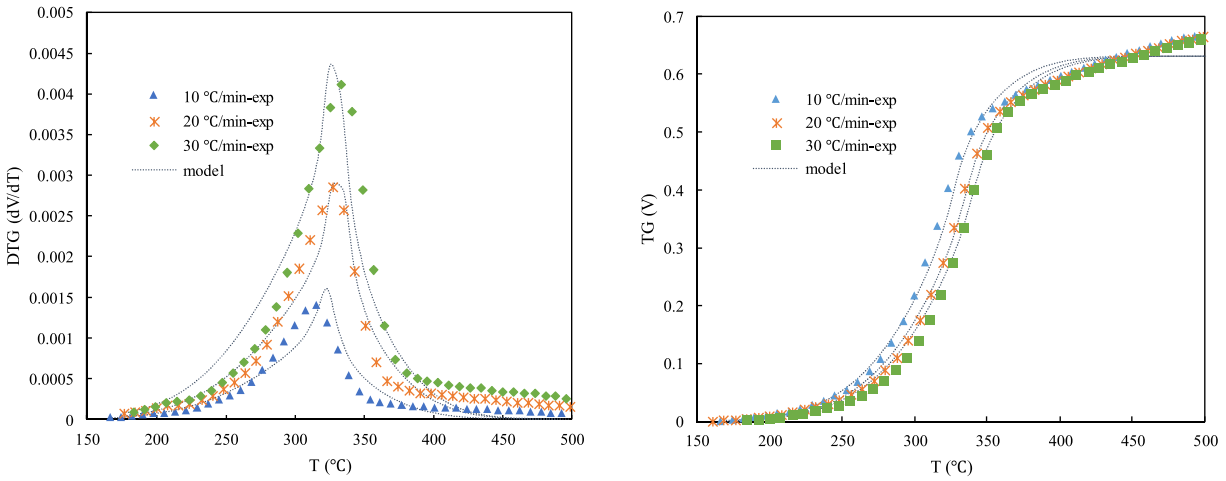

(a) Little Bluestem grass (live)

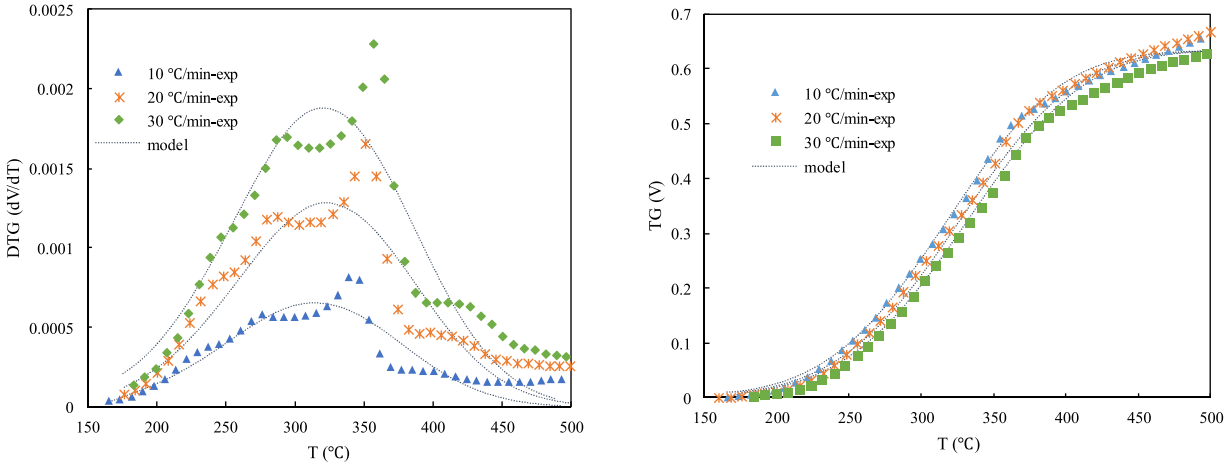

(b) Water oak (live)

Fig. 5. Comparison of best-fit single-reaction DAE model (lines) with TGA and DTG data (points) for a) live little bluestem grass and b) water oak at heating rates of 10, 20 and 30 °C min^{-1}.

Table 3
Kinetic parameters (mean values of three replicates) obtained from the single-reaction DAE model for each plant species (the 90 % confidence intervals are reported in the parentheses).

Species	E_a (kJ mol^{-1})		Log_{10} A (s^{-1})		σ_E (kJ mol^{-1})		V_∞ (normalized)	
	Live	Dead	Live	Dead	Live	Dead	Live	Dead
Darrow's blueberry	163.4(5.5)	163.8(3.6)	21.80(1.21)	21.60(1.28)	24.4(1.7)	15.5(1.4)	0.68(0.06)	0.66(0.07)
Dwarf palmetto	198.6(4.8)	201.9(3.6)	23.46(1.30)	23.59(1.22)	20.7(0.8)	18.9(0.5)	0.63(0.06)	0.66(0.02)
Fetterbush	212.4(5.1)	217.7(3.8)	17.46(1.49)	18.72(1.50)	14.8(0.6)	19.0(0.4)	0.65(0.03)	0.65(0.03)
Inkberry	175.5(3.8)	178.5(2.7)	18.56(1.26)	18.28(1.15)	17.3(1.2)	4.5(0.7)	0.66(0.03)	0.66(0.03)
Live oak	183.3(5.5)	182.9(4.3)	20.17(1.30)	20.63(2.00)	15.8(1.4)	19.4(0.8)	0.58(0.04)	0.59(0.02)
Little bluestem grass	213.1(4.5)	215.3(4.1)	19.52(2.14)	19.91(1.03)	11.5(2.2)	15.2(1.4)	0.61(0.05)	0.61(0.02)
Longleaf pine foliage	223.5(5.9)	220.5(6.1)	21.17(2.20)	21.85(1.02)	11.7(2.1)	12.5(2.5)	0.67(0.03)	0.64(0.03)
Longleaf pine litter	–	239.6(5.7)	–	14.63(1.06)	–	13.9(0.6)	–	0.66(0.02)
Saw palmetto	270.1(4.8)	266.7(3.9)	18.04(1.13)	18.23(2.25)	28.9(2.4)	15.3(1.4)	0.57(0.04)	0.58(0.05)
Sparkleberry	185.6(3.3)	180.1(5.3)	19.18(1.09)	19.72(1.13)	13.4(2.7)	14.8(1.4)	0.60(0.02)	0.59(0.07)
Swamp bay	201.7(6.1)	200.2(2.8)	18.81(1.27)	19.18(1.06)	7.6(2.2)	19.0(1.8)	0.64(0.09)	0.65(0.07)
Water oak	169.9(2.8)	169.8(2.2)	16.93(1.03)	17.61(2.01)	14.2(2.9)	26.4(5.0)	0.64(0.03)	0.64(0.05)
Wax myrtle	212.4(5.3)	217.7(1.8)	22.19(2.16)	22.54(2.10)	22.3(3.5)	15.6(2.6)	0.55(0.02)	0.52(0.08)
Wire Grass	219.0(5.9)	216.0(2.1)	17.83(1.15)	17.74(1.43)	11.8(2.5)	8.0(1.0)	0.67(0.05)	0.65(0.02)
Yaupon	123.7(5.8)	129.1(2.1)	19.51(1.49)	19.93(1.44)	8.7(0.9)	8.2(2.6)	0.59(0.02)	0.59(0.03)

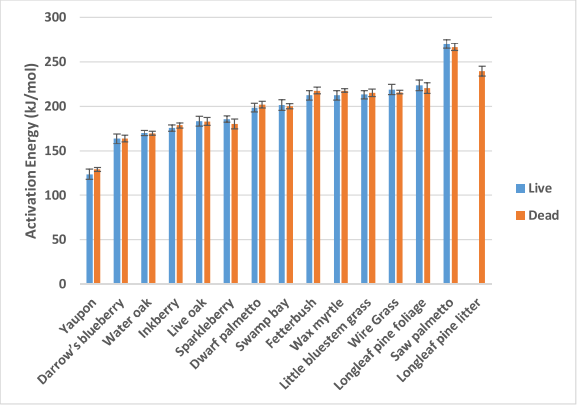

Fig. 6. Comparison of activation energies from the DAE model curve-fit with TG and DTG curves at heating rates of 10, 20, and 30 °C min^{-1}. Error bars represent the 90 % confidence intervals. Activation energies are shown in order of the live sample activation energy.

hemicellulose, lignin), there are significant amounts of other components such as proteins, sugars, lipids, starch, etc. [14], which decompose during each reaction. However, it is beyond the scope of this current work to assign reaction kinetics specifically to each component.

Using one set of coefficients for each DAE model reaction (i.e., corresponding to each major peak in the DTG curve), the cumulative mass and the derivative of the mass from all heating rates of 10, 20, and 30 °C min^{-1} were fitted simultaneously for each plant species. Representative curve-fits of the TGA and DTGA data for live little bluestem grass (single peak) and live water oak (multiple peak) using the multiple-reaction DAE (MDAE) model are presented in Fig. 8. The resulting coefficients determined for each plant species are presented in the supplementary material (**Table S4**). A complete set of plots for the resulting fits is shown in the Supplementary Material (**Fig. S3**).The activation energies for the first reaction (R_1) of each species are shown in Fig. 9 for comparison.

According to the fits for the both single and multiple pyrolysis peaks curves, this model worked well for both single and multiple pyrolysis peaks. The model matched the DTG peaks as well as the cumulative TGA data for both single and multiple peak pyrolysis curves. The pyrolysis of both live and dead samples of Darrow's blueberry, fetterbush, live oak, saw palmetto, sparkleberry, wax myrtle, wire grass, and yaupon consisted of four reactions (R_i). Based on previous biomass modeling efforts [4,7,15], R_1 and R_4 are likely attributed to the hemicellulose and lignin decomposition, respectively. Cellulose decomposition is likely attributed to two reactions (R_2 and R_3).

The pyrolysis of little bluestem grass consisted of three reactions of R_1, R_2, and R_3 which were likely attributed to the decomposition of hemicellulose, cellulose and lignin, respectively. The pyrolysis of both live and dead samples of dwarf palmetto, longleaf pine, swamp bay and water oak consisted of five reactions. For these plants, R_1, R_2, and R_5 were likely attributed to the decomposition of extractives, hemicellulose, and lignin, respectively. Cellulose decomposition is thought to occur during the two intermediate reactions (R_3 and R_4).

The pyrolysis of live and dead inkberry consisted of six reactions. R_1 and R_2 were likely attributed to the decomposition of extractives and hemicellulose, respectively. Cellulose decomposition likely occurred during three reactions (R_3, R_4, and R_5). The last reaction (R_6) was likely attributed to the lignin decomposition. Other biomass pyrolysis studies [4,15,48,50] have shown that hemicellulose and extractives are easier to decompose than cellulose, and cellulose is easier to decompose than lignin, which is consistent with other biomass pyrolysis studies.

Comparing the DTG curves for different types of plant species revealed that the pyrolysis behavior was not consistent between species of the same groups. For example, for grass type species, wire grass had

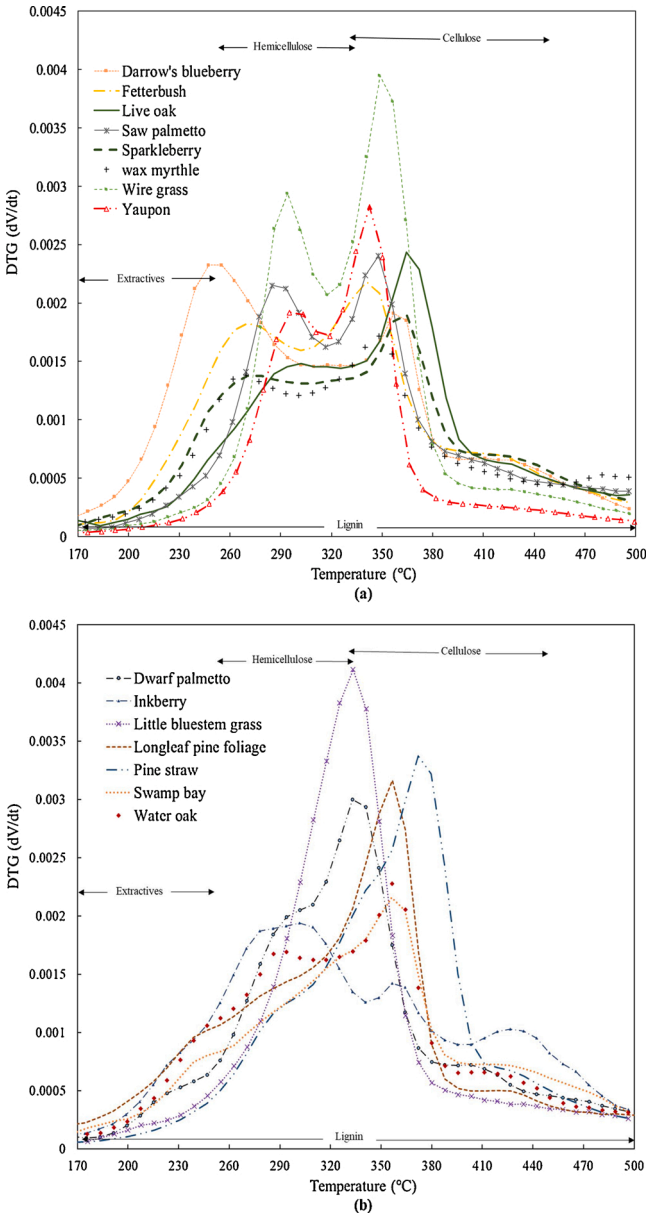

Fig. 7. Measured DTGA pyrolysis curves at a heating rate of 30 °C min^{-1} for (a) Darrow's blueberry, fetterbush, live oak, saw palmetto, sparkleberry, wax myrtle, wire grass and yaupon (b) dwarf palmetto, inkberry, little bluestem grass, longleaf pine, pine straw, swamp bay and water oak. Lines are drawn to connect the data points.

four reactions and little bluestem grass showed three reactions. A similar result was observed for broadleaf species such as inkberry, fetterbush, live oak, water oak, etc. which showed different pyrolysis behaviors. However, palm type species (dwarf palmetto and saw palmetto) showed similar pyrolysis behavior, each with two main peaks.

7. Discussion

The three models used above to find the kinetic parameters of slow pyrolysis reaction of all plant species were the simple one-step model, the single-reaction DAE model, and the multiple-reaction DAE model. The goal was to fit the TGA and DTG data at multiple heating rates in order to provide a model that possibly may be extrapolated to the heating conditions in fires (approximately 100 °C s^{-1}). Fig. 10 shows the comparison of these three models vs. the DTG data for live little bluestem grass (one peak) and live water oak (multiple peaks). The lack of fit

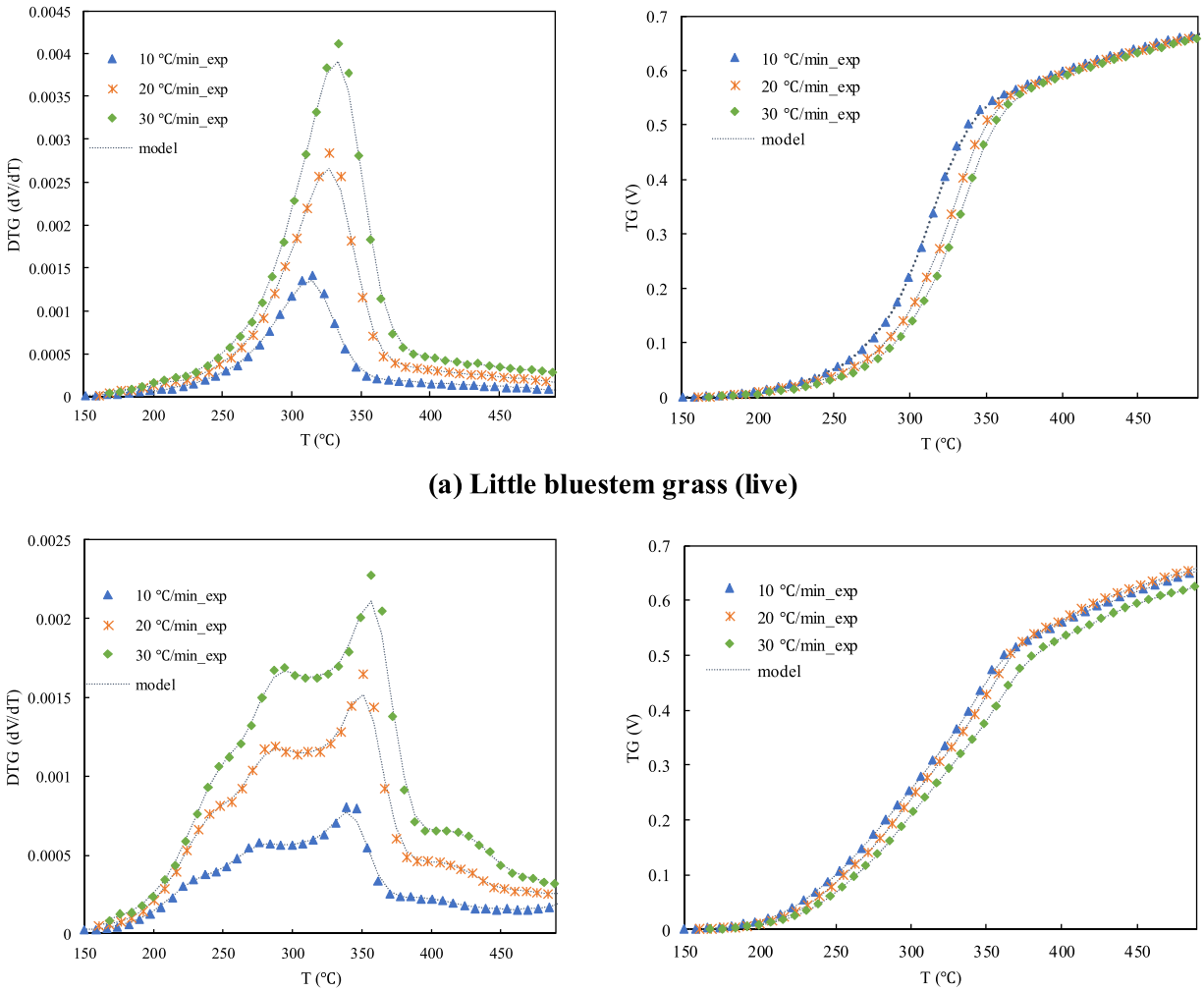

Fig. 8. TG and DTG curves for (a) live little bluestem grass and (b) live water oak resulted from experimental data and multiple-reaction DAE model in heating rates of 10, 20, and 30 °C min^{-1}.

exhibited in Fig. 10**a** by the simple one-step model is because the model was fit to the data from all three heating rates. As expected, this model did not agree well with the data were multiple peaks were observed (Fig. 10b).

The single-reaction DAE model matched the DTG peaks fairly well for the plant species with single peak pyrolysis curves, but not the data with multiple peaks. However, the multiple-reaction DAE model showed the best fit to the experimental data. In particular, the multiple-reaction DAE model is able to describe the slow decay in the reaction rate at temperatures above 375 °C. The multiple-reaction DAE model using the series reaction formulation is not much more complex and almost as fast as the simple first-order model and should be useful over a broader range of heating rates.

To evaluate the quality of the fit between experimental and predicted data and have a quantified comparison between the models, both root mean square error (RMSE) and mean average error (MAE) values corresponding to the simulated datasets in Fig. 10 were calculated, and the results are presented in Table 4. The RMSE and MAE are commonly used together to evaluate the quality of the fit and the variation in the errors of a set of predicted data. The lower values of RMSE and MAE show better fit. The RMSE values are normally equal or greater than the MAE values. The larger the difference between RMSE and MAE values, the larger the variance of errors in the set of predictions. The equal values of RMSE and MAE show that all individual errors are of the same order of magnitude for a given model [43]. As shown in Table 4, the multiple-reaction DAE model had the lowest values of RMSE for both little bluestem grass and water oak, which indicates that this model had the best fit to the experimental data, compared to simple one-step and single-reaction DAE models. The multiple-reaction DAE model had the lowest values of RMSE and MAE for all species by approximately an order of magnitude. For all models, the small difference between RMSE and MAE values indicated that the variance in the errors of individual predicted data was relatively small.

The influence of species on pyrolysis rate is reflected by the comparison of activation energies in Figs. 6,8, and 10. The sort order of activation energies varied slightly for some species with the model chosen. To illustrate this sort order, the activation energies for all of the models for each species were normalized by the average live-species activation energy for that particular model. Results are shown in Fig. 11, along with the average 90% confidence interval for that particular model. Regardless of the model chosen, yaupon had the lowest activation energy, and saw palmetto had the highest activation energy. However, when the first reaction for the MDAE model is compared, it is clear that some species such as wax myrtle and little bluestem grass had a lower first-reaction activation energy than for the other models, and hence changed sort order. The first-reaction activation energy may be related to ignition behavior.

The variation in completion temperatures in live vs. dead samples

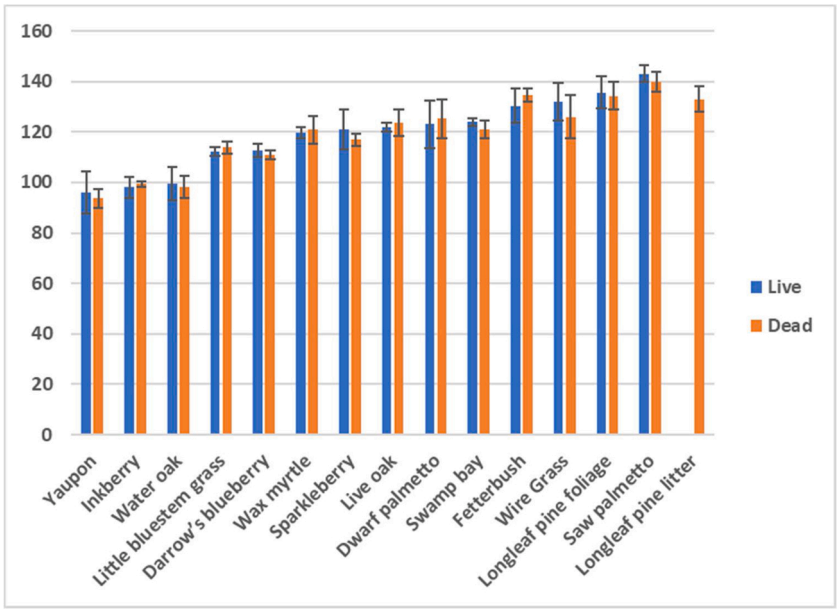

Fig. 9. Comparison of activation energies from the first reaction in the MDAE model curve-fit with TG and DTG curves at heating rates of 10, 20, and 30 °C min^{-1}. Error bars represent the 90 % confidence intervals. Activation energies are shown in order of the live sample activation energy.

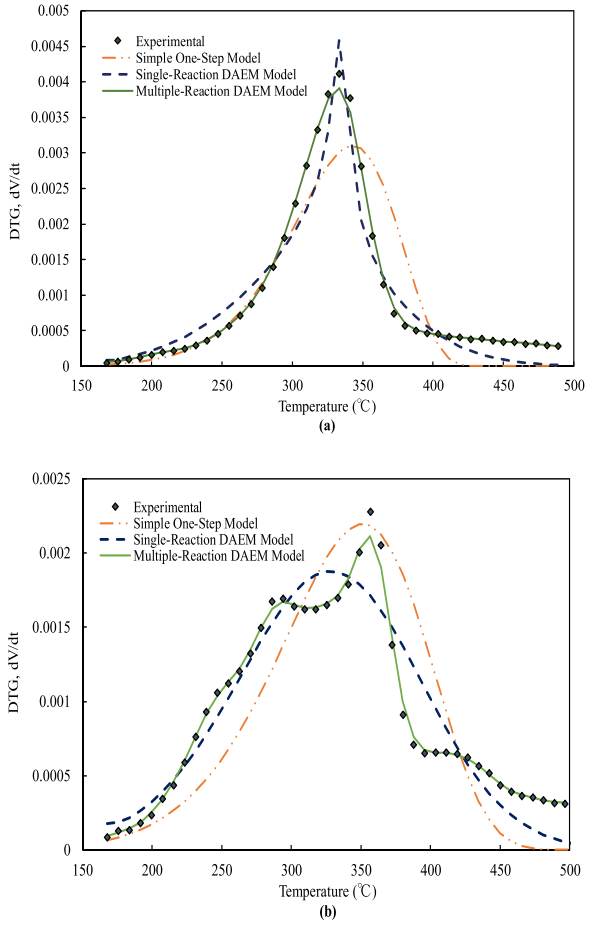

Fig. 10. Comparison of best-fit simple one-step model, single-reaction DAE model, and multiple-reaction DAE model with DTG data for (a) live little bluestem grass and (b) live water oak at heating rate of 30 °C min^{-1}.

Table 4
RMSE and MAE values corresponding to the curve fits of the TGA pyrolysis data at 30 °C min^{-1} for 14 live plant species.

plant	Simple One-Step Model		Single-Reaction DAE model		Multiple-Reaction DAE model	
	RMSE	MAE	RMSE	MAE	RMSE	MAE
Little bluestem grass	5.2×10^{-4}	4.6×10^{-4}	2.5×10^{-4}	2.1×10^{-4}	5.9×10^{-5}	5.5×10^{-5}
Water oak	3.9×10^{-4}	3.2×10^{-4}	2.3×10^{-4}	1.8×10^{-4}	4.6×10^{-5}	4.9×10^{-5}

shown in Fig. 2 is not reflected in the live vs. dead activation energies for any of the above-mentioned models. The reason for this lack of correlation is not readily apparent. In higher heating rate experiments, the tar and light gas yields were shown to be statistically different between the live and dead samples [24,51], which may be part of the explanation for why the completion temperature does not directly correlate with the activation energy.

A simple attempt to compare the activation energies obtained from multiple-reaction DAEM model for each plant species with the corresponding contents of cellulose, hemicellulose and lignin [26]. No significant statistical correlation was observed between cellulose, hemicellulose and lignin content and the corresponding activation energies. However, a more rigorous statistical treatment is suggested before a definite conclusion can be made in this regard.

8. Conclusion

In this study, previously-reported slow-heating pyrolysis data of 14 plant species were analyzed. Pyrolysis completion temperatures, which may be related to combustion rate, were found for all plant species. Each plant species had a different completion temperature, differing by as much as 100 °C. Increasing heating rate increased the completion temperature.

Three different models (the single-reaction first-order model and the single and multiple reaction DAE models) were used to fit the TGA pyrolysis data. The series form of the DAE model was used which greatly reduced computational time. The mass loss and derivative mass loss data

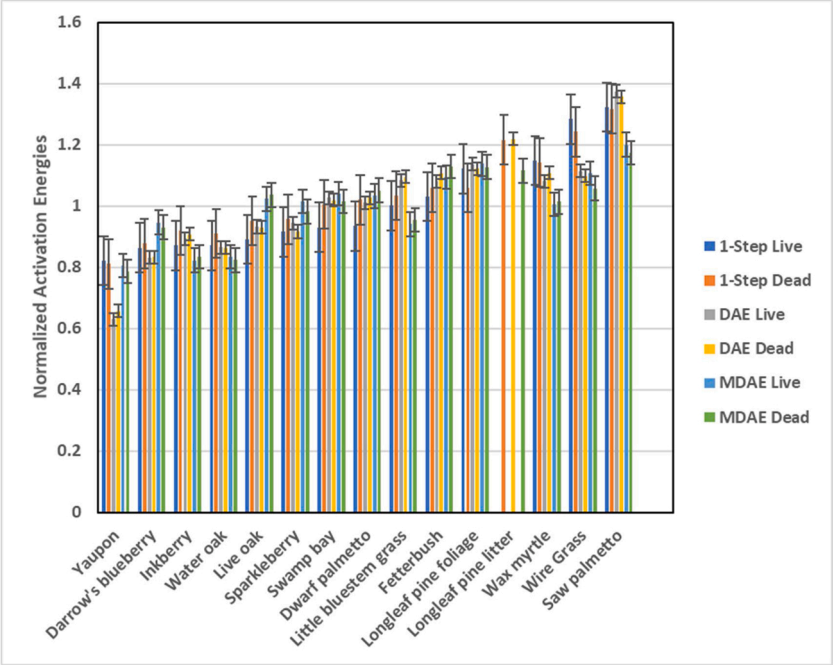

Fig. 11. Normalized activation energies for the different models for each species. Normalization was by the mean live activation energy for that particular model. Error bars are the mean normalized 90 % confidence interval for that model. Data are in the same sort order as the 1-step live model results.

at three heating rates of 10, 20, and 30 °C min^{-1} were fitted simultaneously to find kinetic coefficients for these model forms.

The simple one-step model was not able to reasonably fit the mass loss data over the range of heating rates with one combined set of rate coefficients, nor was it able to match the multiple peaks observed in the DTGA data. The single-reaction DAE model was able to reasonably fit the pyrolysis data for some plant species with only one pyrolysis peak over all three heating rates, although many species had multiple peaks in the DTGA curves. The multiple-reaction DAE model fit the experimental data very well at all heating rates using 3–5 parallel reactions.

Pyrolysis rates of live vs. dead (i.e., air-dried) species did not show significant differences, as indicated by the activation energies of each model. Yaupon had the lowest activation energy for all of the models [1], and saw palmetto had the highest activation energy for all the models. The sort order of activation energies did not change much with model form, except for two species.

Author statement

The roles of each author are stated below:

Elham Amini: Conceptualization, Methodology, Investigation, Software, Data Curation, Writing - Original Draft; Mohammad-Saeed Safdari: Writing - Review & Editing; Nathan Johnson: Investigation, Data Curation; David R. Weise: Writing - Review & Editing, Funding acquisition; Thomas H. Fletcher: Conceptualization, Methodology, Software, Data Curation, Writing - Review & Editing, Project administration

Declaration of Competing Interest

The authors report no declarations of interest.

Acknowledgements

This research was funded by DOD/EPA/DOE Strategic Environmental Research and Development Program ProjectRC-2640, funded through contract 16-JV-11272167-024, administered by the USDA Forest Service PSW Research Station.

Appendix A. Supplementary data

Supplementary material related to this article can be found, in the online version, at doi:https://doi.org/10.1016/j.jaap.2021.105167.

References

[1] T.A. Waldrop, S.L. Goodrick, Introduction to Prescribed Fires in Southern Ecosystems, Report No. SRS-054, U.S.Department of Agriculture Forest Service, Southern Research Station, Asheville, NC, 2012, pp. 1–80 (Slightly Revised 2018) http://www.treesearch.fs.fed.us/pubs/41316.

[2] D.V. Sandberg, C.L. Riccardi, M.D. Schaaf, Reformulation of Rothermel's wildland fire behaviour model for heterogeneous fuelbedsThis article is one of a selection of papers published in the Special Forum on the Fuel Characteristic Classification System, Can. J. For. Res. 37 (2007) 2438–2455, https://doi.org/10.1139/X07-094.

[3] S. Sunphorka, B. Chalermsinsuwan, P. Piumsomboon, Artificial neural network model for the prediction of kinetic parameters of biomass pyrolysis from its constituents, Fuel 193 (2017) 142–158, https://doi.org/10.1016/j.fuel.2016.12.046.

[4] J. Cai, W. Wu, R. Liu, G.W. Huber, A distributed activation energy model for the pyrolysis of lignocellulosic biomass, Green Chem. 15 (2013) 1331–1340, https://doi.org/10.1039/C3GC36958G.

[5] S.A. El-Sayed, M.E. Mostafa, Pyrolysis characteristics and kinetic parameters determination of biomass fuel powders by differential thermal gravimetric analysis (TGA/DTG), Energy Convers. Manage. 85 (2014) 165–172, https://doi.org/10.1016/j.enconman.2014.05.068.

[6] G. Ozsin, A.E. Putun, Kinetics and evolved gas analysis for pyrolysis of food processing wastes using TGA/MS/FT-IR, Waste Manag. 64 (2017) 315–326, https://doi.org/10.1016/j.wasman.2017.03.020.

[7] S.D. Stefanidis, K.G. Kalogiannis, E.F. Iliopoulou, C.M. Michailof, P.A. Pilavachi, A. A. Lappas, A study of lignocellulosic biomass pyrolysis via the pyrolysis of cellulose, hemicellulose and lignin, J. Anal. Appl. Pyrolysis 105 (2014) 143–150, https://doi.org/10.1016/j.jaap.2013.10.013.

[8] F. Richter, G. Rein, Pyrolysis kinetics and multi-objective inverse modelling of cellulose at the microscale, Fire Saf. J. 91 (2017) 191–199, https://doi.org/10.1016/j.firesaf.2017.03.082.

[9] V. Tihay, P. Gillard, Comparison of several kinetic approaches to evaluate the pyrolysis of three Mediterranean forest fuels, Int. J. Wildland Fire 20 (2011) 407–417, https://doi.org/10.1071/WF09106.

[10] W.A. Hough, Caloric Value of Some Forest Fuels of the Southern United States, Res. Note SE-120, USDA Forest Service, Southeastern Forest Experiment Station, Asheville, NC, 1969. http://www.treesearch.fs.fed.us/pubs/2778.

[11] W.M. Jolly, R.A. Parsons, A.M. Hadlow, G.M. Cohn, S.S. McAllister, J.B. Popp, R. M. Hubbard, J.F. Negron, Relationships between moisture, chemistry, and ignition of Pinus contorta needles during the early stages of mountain pine beetle attack, For. Ecol. Manage. 269 (2012) 52–59, https://doi.org/10.1016/j.foreco.2011.12.022.

[12] C.W. Philpot, R.W. Mutch, The Seasonal Trends in Moisture Content, Ether Extractives, and Energy of Ponderosa Pine and Douglas-fir Needles, USDA Forest Service, Intermountain Forest and Range Experiment Station, Ogden, UT, 1971. https://archive.org/details/seasonaltrendsin102phil.
[13] D.R. Weise, C.S. Wright, Wildland fire emissions, carbon and climate: characterizing wildland fuels, For. Ecol. Manage. 317 (2014) 26–40, https://doi.org/10.1016/j.foreco.2013.02.037.
[14] F.J. Matt, M.A. Dietenberger, D.R. Weise, Summative and ultimate analysis of live leaves from southern U.S. Forest plants for use in fire modeling, Energy Fuels 34 (2020) 4703–4720, https://doi.org/10.1021/acs.energyfuels.9b04107.
[15] G. Varhegyi, B. Bobaly, E. Jakab, H. Chen, Thermogravimetric study of biomass pyrolysis kinetics. A distributed activation energy model with prediction tests, Energy Fuels 25 (2011) 24–32, https://doi.org/10.1021/ef101079r.
[16] J.D. Engstrom, J.K. Bulter, S.G. Smith, L.L. Baxter, T.H. Fletcher, D.R. Weise, Ignition behavior of live California chaparral leaves, Combust. Sci. Technol. 176 (2010) 1577–1591, https://doi.org/10.1080/00102200490474278.
[17] F. Bai, Y. Sun, Y. Liu, Q. Li, M. Guo, Thermal and kinetic characteristics of pyrolysis and combustion of three oil shales, Energy Convers. Manage. 97 (2015) 374–381, https://doi.org/10.1071/WF07121/10.1016/j.enconman.2015.03.007.
[18] M.V. Kök, M.R. Pamir, Non-isothermal pyrolysis and kinetics of oil shales, J. Therm. Anal. Calorim. 56 (1999) 953–958, https://doi.org/10.1023/A:1010107701483.
[19] Y. Du, X. Jiang, G. Lv, X. Ma, Y. Jin, F. Wang, Y. Chi, J. Yan, Thermal behavior and kinetics of bio-ferment residue/coal blends during co-pyrolysis, Energy Convers. Manage. 88 (2014) 459–463, https://doi.org/10.1016/j.enconman.2014.08.068.
[20] M. Radojević, B. Janković, V. Jovanović, D. Stojiljković, N. ManićI, Comparative pyrolysis kinetics of various biomasses based on model-free and DAEM approaches improved with numerical optimization procedure, PLoS One 13 (2018), e0206657, https://doi.org/10.1371/journal.pone.0206657.
[21] Q. Xiong, J. Zhang, F. Xu, G. Wiggins, C. Stuart Daw, Coupling DAEM and CFD for simulating biomass fast pyrolysis in fluidized beds, J. Anal. Appl. Pyrolysis 117 (2016) 176–181, https://doi.org/10.1016/j.jaap.2015.11.015.
[22] E. Amini, M.-S. Safdari, J.T. DeYoung, D.R. Weise, T.H. Fletcher, Characterization of pyrolysis products from slow pyrolysis of live and dead vegetation native to the southern United States, Fuel 235 (2019) 1475–1491, https://doi.org/10.1016/j.fuel.2018.08.112.
[23] M.-S. Safdari, E. Amini, D.R. Weise, T.H. Fletcher, Heating rate and temperature effects on pyrolysis products from live wildland fuels, Fuel 242 (2019) 295–304, https://doi.org/10.1016/j.fuel.2019.01.040.
[24] M.-S. Safdari, M. Rahmati, E. Amini, J.E. Howarth, J.P. Berryhill, M. Dietenberger, D.R. Weise, T.H. Fletcher, Characterization of pyrolysis products from fast pyrolysis of live and dead vegetation native to the Southern United States, Fuel 229 (2018) 151–166, https://doi.org/10.1016/j.fuel.2018.04.166.
[25] M.-S. Safdari, E. Amini, D.R. Weise, T.H. Fletcher, Comparison of pyrolysis of live wildland fuels heated by radiation vs. convection, Fuel 268 (2020), https://doi.org/10.1016/j.fuel.2020.117342.
[26] E. Amini, Characterization of Slow Pyrolysis Behavior of Live and Dead Vegetation, PhD Dissertation, Brigham Young University, Chemical Engineering Department, 2020.
[27] M.-S. Safdari, Characterization of Pyrolysis Products From Fast Pyrolysis of Live and Dead Vegetation, PhD Dissertation, Brigham Young University, Chemical Engineering Department, 2018.
[28] E. Amini, M.-S. Safdari, D.R. Weise, T.H. Fletcher, Pyrolysis kinetics of live and dead wildland vegetation from the southern United States, J. Anal. Appl. Pyrolysis 142 (2019), https://doi.org/10.1016/j.jaap.2019.05.002.
[29] M.A. Melvin, National Prescribed Fire Use Survey Report, I. Coalition of Prescribed Fire Councils, 2015. http://stateforesters.org/sites/default/files/publication-documents/2015%20Prescribed%20Fire%20Use%20Survey%20Report.pdf.
[30] H.H. Chapman, Some further relations of fire to longleaf pine, J. For. 30 (1932) 602–604, https://doi.org/10.1093/jof/30.5.602.
[31] M.C.P. Sheffield, J.L. Gagnon, S.B. Jack, D.J. McConville, Phenological patterns of mature longleaf pine (Pinus palustris Miller) under two different soil moisture regimes, For. Ecol. Manage. 179 (2003) 157–167, https://doi.org/10.1016/S0378-1127(02)00523-6.
[32] A.A. Boateng, P.L. Mtui, CFD modeling of space-time evolution of fast pyrolysis products in a bench-scale fluidized-bed reacto, Appl. Therm. Eng. 33-34 (2012) 190–198, https://doi.org/10.1016/j.applthermaleng.2011.09.034.
[33] Q. Xue, D. Dalluge, T.J. Heindel, R.O. Fox, R.C. Brown, Experimental validation and CFD modeling study of biomass fast pyrolysis in fluidized-bed reactors, Fuel 97 (2012) 757–769, https://doi.org/10.1016/j.fuel.2012.02.065.
[34] M. Chaos, M.M. Khan, N. Krishnamoorthy, J.L. De Ris, S.B. Dorofeev, Evaluation of optimization schemes and determination of solid fuel properties for CFD fire models using bench-scale pyrolysis tests, Proc. Combust. Inst. 33 (2011) 2599–2606, https://doi.org/10.1016/j.proci.2010.07.018.
[35] V. Vand, A theory of the irreversible electrical resistance changes of metallic films evaporated in vacuum, Proc. Phys. Soc. 55 (1943) 222–246, https://doi.org/10.1088/0959-5309/55/3/308.
[36] A. Soria-Verdugo, N. Garcia-Hernando, L.M. Garcia-Gutierrez, U. Ruiz-Rivas, Analysis of biomass and sewage sludge devolatilization using the distributed activation energy model, Energy Convers. Manage. 65 (2013) 239–244, https://doi.org/10.1016/j.enconman.2012.08.017.
[37] A.P. Richards, T.H. Fletcher, A comparison of simple global kinetic models for coal devolatilization with the CPD model, Fuel 185 (2016) 171–180, https://doi.org/10.1016/j.fuel.2016.07.095.
[38] D.K. Shen, S. Gu, B. Jin, M.X. Fang, Thermal degradation mechanisms of wood under inert and oxidative environments using DAEM methods, Bioresour. Technol. 102 (2011) 2047–2052, https://doi.org/10.1016/j.biortech.2010.09.081.
[39] D.B. Anthony, J.B. Howard, H.C. Hottel, H.P. Meissner, Rapid devolatilization of pulverized coal, Symp. (Int.) Combus. 15 (1975) 1303–1317, https://doi.org/10.1016/S0082-0784(75)80392-4.
[40] T.H. Fletcher, A.R. Kerstein, R.J. Pugmire, M.S. Solum, D.M. Grant, Chemical percolation model for devolatilization .3. Direct use of C-13 NMR data to predict effects of coal type, Energy Fuels 6 (1992) 414–431, https://doi.org/10.1021/ef00034a011.
[41] T.H. Fletcher, Review of 30 years of research using the chemical percolation devolatilization model, Energy Fuels 33 (2019) 12123–12153, https://doi.org/10.1021/acs.energyfuels.9b02826.
[42] D.M. Grant, R.J. Pugmire, T.H. Fletcher, A.R. Kerstein, Chemical model of coal devolatilization using percolation lattice statistics, Energy Fuels 3 (1989) 175–186, https://doi.org/10.1021/ef00014a011.
[43] E. Torres-Garcia, P. Brachi, Non-isothermal pyrolysis of grape marc, J. Therm. Anal. Calorim. 139 (2019) 1463–1478, https://doi.org/10.1007/s10973-019-08530-z.
[44] Td.O. Zuppa Neto, T.G. Avval, P.Ad.O. Morais, W.C. Ellis, S.C. Chapman, A.E. de Oliveira, M.R. Linford, P.B. Farnsworth, N.R. Antoniosi Filho, Direct dielectric barrier discharge ionization promotes rapid and simple lubricant oil fingerprinting, J. Am. Soc. Mass Spectrom. (2020), https://doi.org/10.1021/jasms.0c00071.
[45] R.K. Mishra, K. Mohanty, Pyrolysis kinetics and thermal behavior of waste sawdust biomass using thermogravimetric analysis, Bioresour. Technol. 251 (2018) 63–74, https://doi.org/10.1016/j.biortech.2017.12.029.
[46] J.M. Vleeskens, B.N. Nandi, Burnout of coals: comparative bench-scale experiments on pulverized fuel and fluidized bed combustion, Fuel 65 (1986) 797–802, https://doi.org/10.1016/0016-2361(86)90072-4.
[47] E. Banon, A. Marcilla, A.N. Garcia, P. Martinez, M. Leon, Kinetic model of the thermal pyrolysis of chrome tanned leather treated with NaOH under different conditions using thermogravimetric analysis, Waste Manag. 48 (2016) 285–299, https://doi.org/10.1071/WF07121/10.1016/j.wasman.2015.10.012.
[48] Z.Q. Ma, D.Y. Chen, J. Gu, B.F. Bao, Q.S. Zhang, Determination of pyrolysis characteristics and kinetics of palm kernel shell using TGA-FTIR and model-free integral methods, Energy Convers. Manage. 89 (2015) 251–259, https://doi.org/10.1071/WF07121/10.1016/j.enconman.2014.09.074.
[49] J. Hillier, T. Bezzant, T.H. Fletcher, Improved method for the determination of kinetic parameters from non-isothermal thermogravimetric analysis (TGA) data, Energy Fuels 24 (2010) 2841–2847, https://doi.org/10.1021/ef1001265.
[50] J. Cai, W. Wu, R. Liu, Sensitivity analysis of three-parallel-DAEM-reaction model for describing rice straw pyrolysis, Bioresour. Technol. 132 (2013) 423–426, https://doi.org/10.1016/j.biortech.2012.12.073.
[51] D.R. Weise, T.H. Fletcher, M.-S. Safdari, E. Amini, J. Palarea-Albaladejo, Application of compositional data analysis to determine the effects of heating mode, moisture status and plant species on pyrolysates, Int. J. Wildland Fire (2021), https://doi.org/10.1071/WF20126. In press.